International Journal of Mass Spectrometry 300 (2011) 149–157

Contents lists available at ScienceDirect

International Journal of Mass Spectrometry

journal homepage: www.elsevier.com/locate/ijms

Characterization of naphthenic acids in crude oils and naphthenates by electrospray ionization FT-ICR mass spectrometry

Mmilili M. Mapolelo[a], Ryan P. Rodgers[b,*,1], Greg T. Blakney[b], Andrew T. Yen[c,2], Sam Asomaning[c], Alan G. Marshall[b,**,1]

[a] Department of Chemistry and Biochemistry, Florida State University, Tallahassee, FL 32306, USA
[b] Ion Cyclotron Resonance Program, National High Magnetic Field Laboratory, Florida State University, 1800 East Paul Dirac Drive, Tallahassee, FL 32310-4005, USA
[c] Baker Hughes, 12645W. Airport Boulevard, Sugar Land, TX 77478, USA

ARTICLE INFO

Article history:
Received 8 April 2010
Received in revised form 2 June 2010
Accepted 3 June 2010
Available online 16 June 2010

Keywords:
Fourier transform
Ion cyclotron resonance
FTMS
Petroleum

ABSTRACT

We present the selective ionization of acidic components of crude oils and naphthenates by negative-ion electrospray ionization (ESI) Fourier transform ion cyclotron resonance mass spectrometry (FT-ICR MS). We further characterize isolated naphthenic acids from a calcium napthenate deposit by negative-ion ESI tandem mass spectrometry (MS^n): collision-induced dissociation (CID) and infrared multiphoton dissociation (IRMPD). Selective ionization by electrospray affords direct characterization of neutral nitrogen species and naphthenic acids in petroleum without derivatization or preconcentration of the sample, and with minimal sample consumption. Acids isolated from a calcium naphthenate deposit are tetraprotic with a C_{80} hydrocarbon skeleton; commonly known as "ARN" acids, whereas sodium naphthenate consists of low molecular weight (C_{15} to C_{35}) linear saturated monoprotic carboxylic acids. IRMPD and CID fragmentation of ARN acids result in both dehydration and decarboxylation of the carboxylic acid groups without dealkylation. However, CID produced more extensive fragmentation leading to dealkylation of the hydrocarbon skeleton. The ultrahigh resolution and mass accuracy of FT-ICR MS and MS/MS provide for detailed identification and compositional differences of acidic species in crude oils and naphthenates, and also afford structural characterization of acids isolated from naphthenate deposits.

1. Introduction

1.1. Petroleum crude oil and bitumen

Biodegraded oils dominate the world petroleum inventory, with the largest reserves found not in the Middle East, but in the Americas [1]. Biodegraded oils also represent a significant fraction of petroleum in conventional oil reserves found in Africa, Canada, South America, and the Gulf of Mexico [1]. Petroleum crude oils are typically composed of ~85–90% hydrocarbons (C_cH_h) and ~10–15% polar and slightly polar species [2]. The polar species contain heteroatoms ($N_nO_oS_s$) and metals (vanadium (V), iron (Fe), nickel (Ni)) [2]. Most biodegraded oils are significantly enriched in polar compounds. The polar fraction in petroleum liquids is the most problematic with respect to pollution, fouling of catalysts, corrosion, formation of deposits, and emulsions during production and processing [3–5].

1.2. Naphthenates

Recently, more and more oilfields face severe flow assurance problems due to formation of deposits and soaps, generally termed naphthenates [6–8]. Naphthenate deposition occurs mainly during upstream operations, commonly at the oil/water cutoff point. The consequent obstruction of pipelines, frequent unscheduled shutdowns, and physical clean-up periods during maintenance operations reduce productivity [9–12]. The naphthenate deposition problem has become more prevalent as new crude oil reservoirs contain immature, heavy crude oils with higher heteroatom content, that are also biodegraded and have thereby lost saturated hydrocarbons and waxes and built up higher naphthenic acid content [13–17]. Offshore production installations in Great Britain and Norway (North Sea), West Africa (Gulf of Guinea; Angola, Cameroon, Gabon and Nigeria) the North West Shelf of Australia, South East Asia (South China Sea, Malaysia, Vietnam, Bohai Bay in China and Kutei Basin in Indonesia) and Gulf of Mexico

* Corresponding author. Tel.: +1 850 644 2398; fax: +1 850 644 1366.
** Corresponding author. Tel.: +1 850 644 0529; fax: +1 850 644 1366.
E-mail addresses: rodgers@magnet.fsu.edu (R.P. Rodgers), marshall@magnet.fsu.edu (A.G. Marshall).
[1] Also a member of the Department of Chemistry, Florida State University, 95 Chieftain Way, Tallahassee, FL 32306, USA.
[2] Current address: Nalco Energy Service, 7705 Highway 90-A Sugar Land, TX 77478, USA.

1387-3806/$ – see front matter © 2010 Elsevier B.V. All rights reserved.
doi:10.1016/j.ijms.2010.06.005

have reported unprecedented naphthenate deposition problems [8,10,16].

Naphthenate deposition occurs during pressure reduction, during which degassing of the carbon dioxide from the production water results in an increased pH and dissociation of naphthenic acids at the oil/water interface [10,18]. During the process naphthenic acid hydrolysis occurs and the carboxylate groups react with inorganic cations in production waters, and metal naphthenates precipitate [18,19]. Two main types of naphthenates are known to form in production fluids: calcium naphthenate solids that occur as sticky or hardened deposits, and sodium naphthenate emulsions that can form tight emulsions as soaps or sludge [8]. Calcium and sodium naphthenates are formed by the interaction of naphthenic acids and divalent ions (Ca^{2+}, Fe^{2+} and Mg^{2+}) or monovalent (Na^+, K^+) ions in production waters. They occlude silica/sand, mineral scales, iron hydroxide/oxides and sulfides, clay, mud residues (bentonites), flocculated asphaltenes, resins, and treating chemicals [17]. The naphthenates and other particles adhere to oil water interfaces and can sometimes become finely dispersed within the water itself. Naphthenates, especially calcium naphthenates can deposit across the oil process system from wellheads, subsea flowlines, oil/water separators, electrostatic treaters/coalescers, heat exchanger tubes and even within oil storage tanks [6]. Crude oils that form sodium naphthenates are often enriched in naphthenic acids [8,10] and other acidic heteroatomic species whereas those that form calcium naphthenate deposits are also enriched in naphthenic acids, asphaltenes and other acidic heteroatomic species [8]. Such crude oils have a tendency to be severely biodegraded, which means that their wax and saturates fractions have been depleted with creation of naphthenic acids, resulting in an increase in total acid number [20].

1.3. Electrospray ionization for petroleum characterization

The introduction of electrospray ionization (ESI) in the late 1980s [21,22] opened a new frontier for characterization of polar molecules in petroleum and petroleum derived materials. Zhan and Fenn showed that most of the polar constituents in fossil fuels such as petroleum and petroleum derived materials (e.g., crude oil, jet fuel and gasoline) are easily ionized by electrospray and easily detected by low resolution mass spectrometry [23]. Fenn's paper launched a flood of publications in which ESI was coupled to various mass analyzers, of which Fourier transform ion cyclotron resonance (FT-ICR) mass spectrometers has yielded the most remarkable results in the compositional analysis of petroleum and related materials.

ESI is a "soft" ionization technique that selectively generates quasimolecular ions at atmospheric pressure with minimal or no fragmentation of the analyte [21,22]. ESI typically generates positively charged ions by protonation of basic species and negatively charged ions by deprotonation of acidic species. Fragmentation is especially problematic for a complex sample such as petroleum, because generation of more than one signal per analyte can greatly complicate an already crowded mass spectrum [3–5,23]. ESI has gained popularity because: (i) at a flow rate of 4–400 nL/min, sample consumption is minimal (~10 pmol); (ii) multiple charges [24,25] can lower the m/z to 500–2000 (i.e., the m/z range for quadrupole and ion trap mass analyzers) for even very large molecules (>100,000 Da) down to the m/z range of common mass analyzers; [21,26] (iii) ESI selectively favors ionization of polar species (e.g., acidic or basic species in a petroleum sample); (iv) ESI is easily coupled to various mass analyzers; and (v) chemical pre-treatment of the analyte is often not necessary.

In conventional ESI, basic species are protonated with a weak acid such as formic acid (HCOOH) or acetic acid (CH_3COOH) to form $[M+H]^+$ ions, whereas acidic species are deprotonated with a weak base such as ammonium hydroxide (NH_4OH) to form $[M-H]^-$ ions. For example, positive-ion electrospray selectively ionizes basic nitrogen (e.g., pyridine homologues), some primary amines, and sulfoxide species from petroleum. Basic nitrogen compounds deactivate hydrotreatment catalysts used for sulfur removal and also increase fuel instability during storage [27,28]. In addition, nitrogen oxides (N_nO_o) and sulfur oxides (O_oS_s) that are released during combustion of petroleum and its products are the two major atmospheric pollutants generally believed to be precursors of acid rain and photochemical smog [29]. Negative-ion electrospray of petroleum selectively ionizes carboxylic ("naphthenic") acids, phenols and "neutral nitrogen" species (e.g., pyrrole homologues). Naphthenic acid compositions range from saturated to acyclic, aromatic, and polyaromatic acids [30]. These organic acids are responsible for liquid phase corrosion in crude oil transport through pipelines and in refinery processing [31], and are also associated with formation of emulsions and naphthenate deposits that cost the petroleum industry millions of dollars annually in "flow assurance" problems [10].

Positive- and negative-ion electrospray can access species containing one or more heteroatoms ($N_nO_oS_s$), as from heavy crude oils. Furthermore, species that are not accessible by direct electrospray can be rendered ESI-observable by chemical derivatization. For example, sulfur in non-polar sulfides, thiophenes, and polycyclic aromatic sulfur heterocycles (PASHs) can be pre-isolated with a palladium (II) containing column and methylated or phenylated to yield methyl or phenyl thiophenium cations that are already present as ions in solution before electrospray [32,33]. Methylation also enables electrospray ionization of furans (oxonium ions) and aromatic hydrocarbons [33]. The major limitation of ESI for

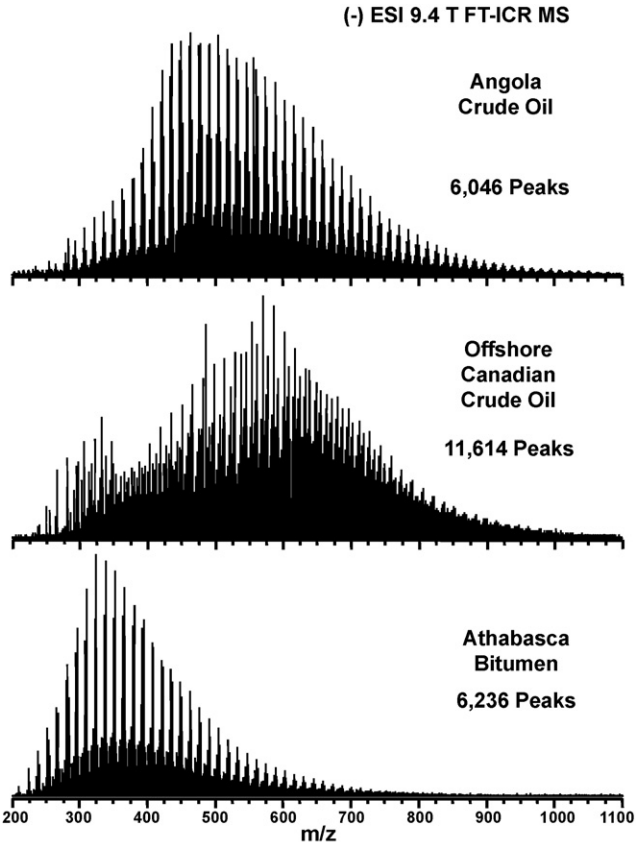

Fig. 1. Broadband negative-ion electrospray 9.4 T FT-ICR mass spectra for three crude oils of different geographical origin. The number of assigned peaks with magnitude atleast 6 times the baseline rms noise for the three crudes is 6046, 11,614 and 6236. The average mass resolving power, $m/\Delta m_{50\%}$, ranged from 550,000 to 840,000 for each crude.

petroleum mass analysis is that it cannot efficiently ionize most of the hydrocarbons that make the bulk of the remaining 85–90% of petroleum and petroleum derived materials [5]. Furthermore, the efficiency of ESI for generation of ions depends strongly on spray conditions and physical properties of analytes such as pK_a, hydrophobicity, and surface activity [34,35].

No single ionization method produces ions from chemically different neutrals with comparable efficiency. Here, we show that polar species in petroleum and related products, ranging from weakly acidic molecules such as pyrrolic nitrogen compounds, as well as more strongly acidic molecules such as carboxylic acids (naphthenic acids), can be selectively ionized by negative-ion electrospray. Negative-ion electrospray thus provides access to the most problematic components of petroleum, to molecular level characterization of complex mixtures previously characterized only from their bulk properties.

2. Materials and methods

2.1. Samples

Angola and offshore Canadian crude oils and Athabasca bitumen were used as supplied. The sodium and calcium naphthenate deposits were collected from production separators in which naphthenate deposition had been reported and were used as supplied. HPLC grade methanol and toluene (Fisher Scientific), ammonium hydroxide (20–35% ammonia in water) (Sigma–Aldrich) were used as supplied. Acidic extracts from sodium naphthenate deposit

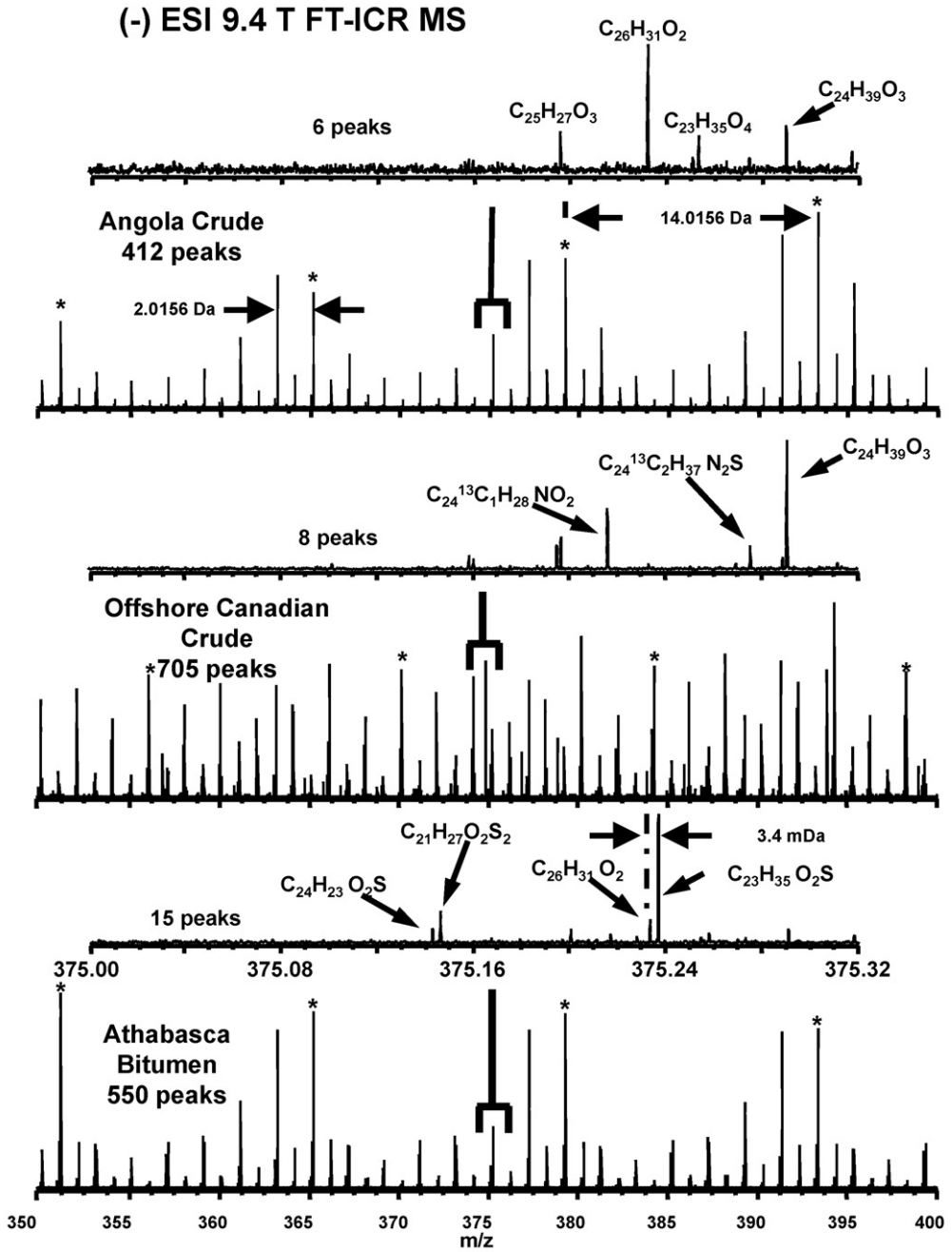

Fig. 2. Mass scale-expanded segments (50 Da and 320 mDa) of the full range mass spectra of the three crudes. High mass accuracy (better than 0.5 ppm) enables unique elemental composition assignments at 375 Da nominal mass. The 50 Da mass segment shows homologous series with 2 and 14 nominal mass spacings. The starred peaks (*) are 14 Da apart and constitute members of the same homologous series.

from Caribbean crude oil and calcium naphthenate deposit from European crude oil were extracted by use of previously reported extraction methods [36].

2.2. Sample preparation for ESI FT-ICR MS

Sample preparation for the analysis of acidic species in crude oils and naphthenate by negative-ion electrospray FT-ICR MS has been previously reported [36,37]. Samples were analyzed at a concentration of 500 μg/mL in a standard ESI spray mix (50:50 (v:v) toluene:methanol) for mass spectrometric analysis. A representative aliquot (1 mL) of a crude oil sample or acid extract was spiked with 10 μL of 2% ammonium hydroxide (NH_4OH) in methanol to facilitate deprotonation of the acidic species to generate $[M-H]^-$ ions. Each sample was delivered to the mass spectrometer ionization source via a syringe pump at a rate of 400 nL/min through a 50 μm i.d. fused silica microESI needle under typical ESI conditions (2.0 kV; tube lens, 350 V; heated capillary current, 4.20 A) [38].

2.3. Mass analysis

Each sample was analyzed with a custom-built 9.4 T 22 cm horizontal room temperature bore diameter (Oxford Corp., Oxford Mead, UK) FT-ICR mass spectrometer at the National High Magnetic Field Laboratory [39]. A Modular ICR Data Acquisition System (MIDAS) was used to collect and process ICR data [39,40]. Calibrant ions were generated by electrospray of HP mix (Agilent, Palo Alto, CA). Ions were accumulated externally in a linear octopole ion trap for 1–5 s and transferred through rf-only multipoles to a 10 cm diameter, 30 cm long open cylindrical Penning ion trap [41,42]. Octopole ion guides were operated at 2.0 MHz with 100 V_{p-p} rf amplitude and a 900 μs transfer period [43]. Broadband frequency-sweep (chirp) dipolar excitation (~70–641 kHz at a sweep rate of 50 Hz/μs and peak-to-peak amplitude of 190 V_{p-p}) was followed by direct mode image current detection to yield 4 Mword time-domain data. One hundred time-domain data sets were co-added and Hanning apodized, followed by a single zero-fill before fast Fourier transformation and magnitude calculation. Frequency was converted to mass-to-charge ratio by the quadrupolar electrostatic trapping potential approximation [44,45].

Tandem mass spectrometry (MS^n) experiments for structural characterization of acid extracts were performed by both infrared multiphoton dissociation (IRMPD) and collision-induced dissociation (CID). IRMPD experiments were performed with a (Synrad model J48-2 Mukilteo, WA) 40 W continuous-wave CO_2 laser (λ = 10 μm) for 100–800 ms of irradiation at 60% laser power (low) and 90% laser power (high). CID experiments were performed with a hybrid LTQ (ThermoFisher Scientific) 14.5 T FT-ICR mass spectrometer equipped with an ESI source, with spray voltage 2.0–2.5 kV and capillary temperature 275 °C. Optimum collision energy for CID fragmentation varies linearly with m/z. Therefore, in the LTQ mass spectrometer, the collision energy was normalized for each m/z value selected for dissociation (normalized collision energy (NCE)) [46].

2.4. Mass calibration

Mass spectra were frequency-to-m/z calibrated externally with respect to an Agilent #G2421A electrospray "tuning mix", for all peaks with magnitudes of at least six standard deviations above baseline noise. Externally calibrated spectra were then internally recalibrated with respect to the most abundant homologous alkylation series for each sample. All masses were then converted to the Kendrick mass scale [47]. Kendrick-sorted masses were imported into Microsoft Excel for identification by a formula calculator as previously reported [48,49]. In summary, molecular formulas were assigned to peaks of lowest m/z value for each Kendrick Mass Defect (KMD) series. Peaks of higher m/z ratio for the same KMD value were assigned by adding multiples of CH_2 to the molecular formula. Calculations were limited to formulas containing less than 100 ^{12}C, 2 ^{13}C, 200 ^{1}H, 5 ^{14}N, 10 ^{16}O, 3 ^{32}S, and 1 ^{34}S. If more than one possible formula was generated for a specific mass, one or more could almost always be confirmed or eliminated by the presence/absence of a corresponding ^{13}C, ^{18}O, or ^{34}S peak. In this way, ~95% of the peaks could be assigned to a unique chemical formula.

3. Results and discussion

The characterization of polar constituents of crude oil makes it possible to trace petroleum molecules back to their biological precursors [37]. For example, petroleum organic acids (naphthenic acids) serve as a geochemical fingerprint of the original source rock and indicators of crude oil maturity [50,51].

Petroleum and its derivatives are largely composed of homologous series, C_cH_{2c+z} X, in which c is the carbon number, z is the "hydrogen deficiency" index, and X denotes heteroatoms (N, S, O) in each molecule [5,37], and successive members of the series differ by multiples of CH_2. Although hydrogen deficiency provides a measure of aromaticity, each ring or double bond contributes −2, and z = +2 for a fully saturated hydrocarbon. Thus, a more direct index is double bond equivalents (DBE) [52] defined as the number of rings plus double bonds involving carbon for a petrochemical of composition, $C_cH_hN_nO_oS_s$:

$$\text{Double bond equivalents (DBE)} = c - \frac{h}{2} + \frac{n}{2} + 1 \quad (1)$$

The two parameters are related by:

$$z = -2\text{DBE} + n + 2 \quad \text{or equivalently,} \quad \text{DBE} = \frac{-z}{2} + \frac{n}{2} + 1 \quad (2)$$

We begin by presenting the broadband ESI mass spectra of the crude oils to show that the ionization efficiency is not limited by molecular weight or compositional complexity. We then analyze the individual heteroatom classes for the acidic compounds. Each class may then be further sorted according to DBE and number of carbons to reveal patterns of aromaticity and alkylation that define their core structures.

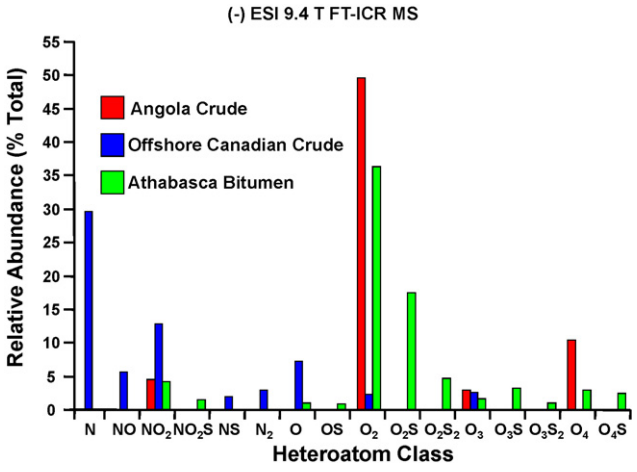

Fig. 3. Heteroatom class distribution for the three crude oils, based on negative-ion electrospray FT-ICR mass spectra. Only classes with relative abundance > 1% are shown.

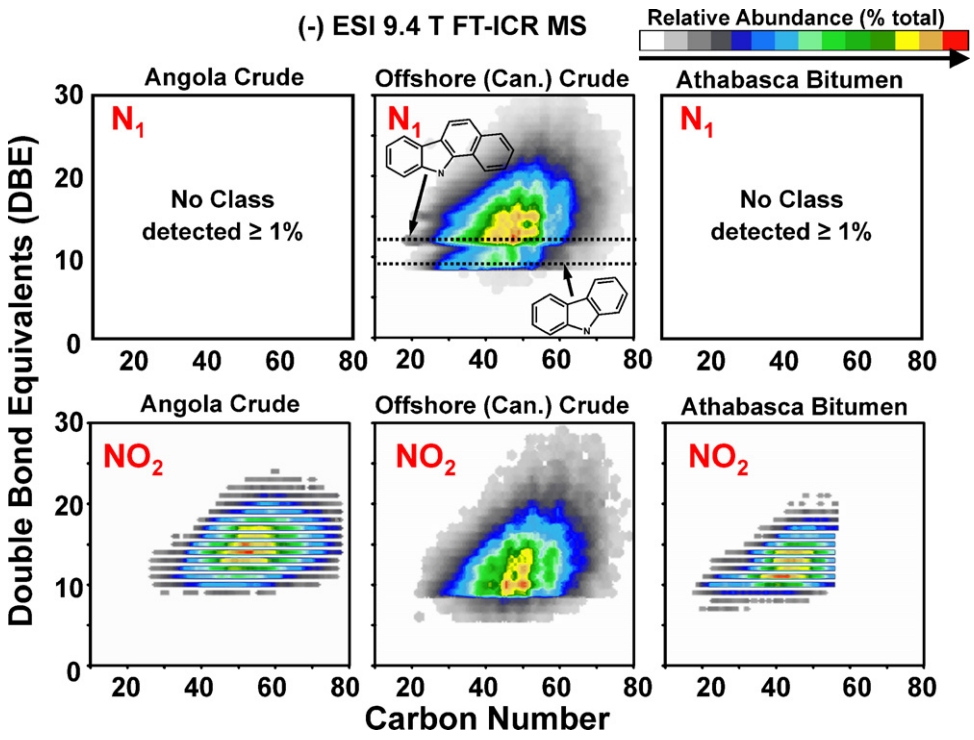

Fig. 4. Relative isoabundance color-contoured plots of double bond equivalents (DBE) vs. carbon number for N and NO_2 class species from the three crude oils. Data derived from negative-ion electrospray FT-ICR mass spectra.

3.1. Crude oil characterization

3.1.1. Mass distribution

Broadband negative-ion electrospray 9.4 T FT-ICR MS identifies thousands of acidic species in two crude oils and bitumen (Fig. 1). Angola crude (6046 peaks) and offshore Canadian crude (11,614 peaks) exhibit similar molecular weight distributions, from 200 to 1100 Da, whereas the Athabasca bitumen (6236 peaks) components have lower masses. The observed molecular weight distributions (200–1000 Da) accord with those previously reported for acidic crude oils by high resolution mass spectrometry [37,53], and are composed mainly of neu-

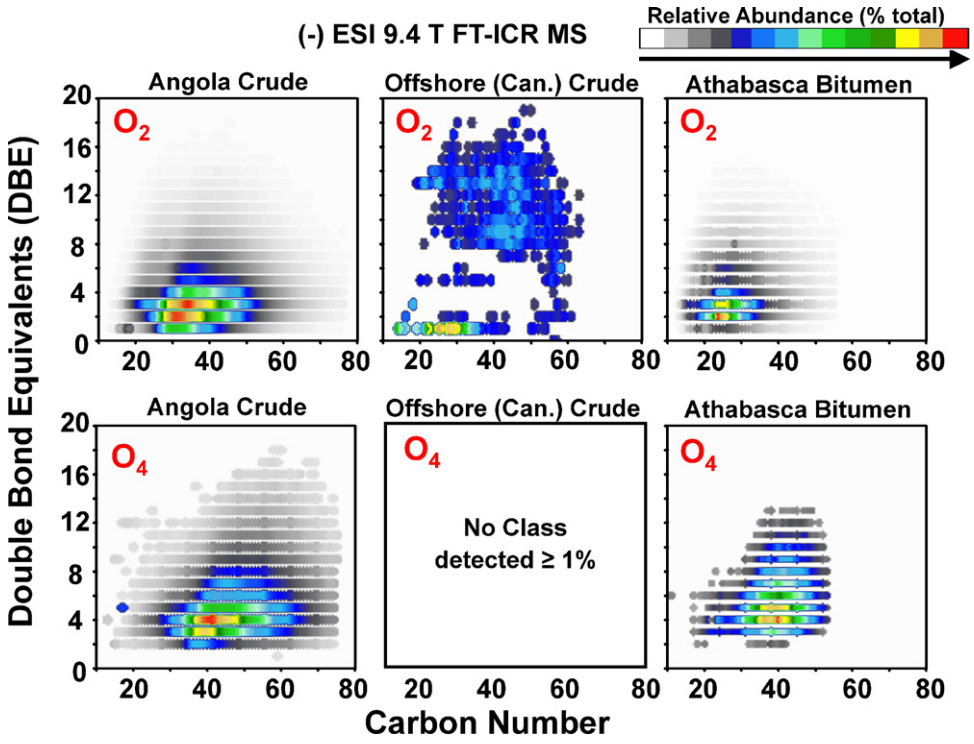

Fig. 5. DBE vs. carbon number images (as in Fig. 4) for O_2 and O_4 class species from the three crude oils.

tral nitrogen, naphthenic acids, and other acidic heteroatomic species.

The importance of ultrahigh mass resolving power and mass accuracy in the determination of compositional differences in crude oils is evident from Fig. 2, which shows 50 Da and 320 mDa mass scale-expanded segments for the three samples, for which the average mass resolving power, $m/\Delta m_{50\%}$, in which $\Delta m_{50\%}$ is mass spectral peak full width at half-maximum peak height, is ~670,000, 550,000 and 840,000. The mass segment from 350 to 400 Da (all species are singly charged, as evident from the unit m/z spacing between species differing by $^{12}C_c$ and $^{13}C_1{}^{12}C_{n-1}$) shows ~2 Da and ~14 Da periodicities characteristic of petroleum, with 412, 705 and 550 peaks (each with magnitude > 6 times the baseline rms noise) from 350 to 400 Da (at an average $m/\Delta m_{50\%}$ = 1,000,000). The asterisks denote members of the same homologous series that differ by multiples of 14 Da (i.e., CH_2) whereas a 2 Da (H_2) spacing arises from compounds that differ by one ring or double bond. The labeled peaks in the 320 mDa mass scale-expanded segment at 375 Da nominal mass were assigned with an average mass error of ~0.1 ppm, for the three samples. The 320 mDa segment at 375 for Athabasca bitumen includes a resolved 3.4 mDa doublet of molecules that differ by $^{12}C_3$ vs. $^{32}SH_4$, essential for identifying sulfur-containing species, and demonstrating the need for ultrahigh mass resolution and accuracy.

3.1.2. Heteroatom class composition

Fig. 3 shows the relative abundance of compounds comprising each heteroatom class ($N_nO_oS_s$) in each of the three samples. Note that the abundances are scaled relative to the highest-magnitude peak in that mass spectrum, so that even if the absolute abundance of a given class is the same for two samples, its relative abundance will depend on differences in absolute abundances of the other species. The heteroatom classes differ dramatically among the three samples. Offshore Canadian crude has the highest content of classes containing neutral nitrogen (N, NO, NO_2, NO_2S, NS, and N_2) but

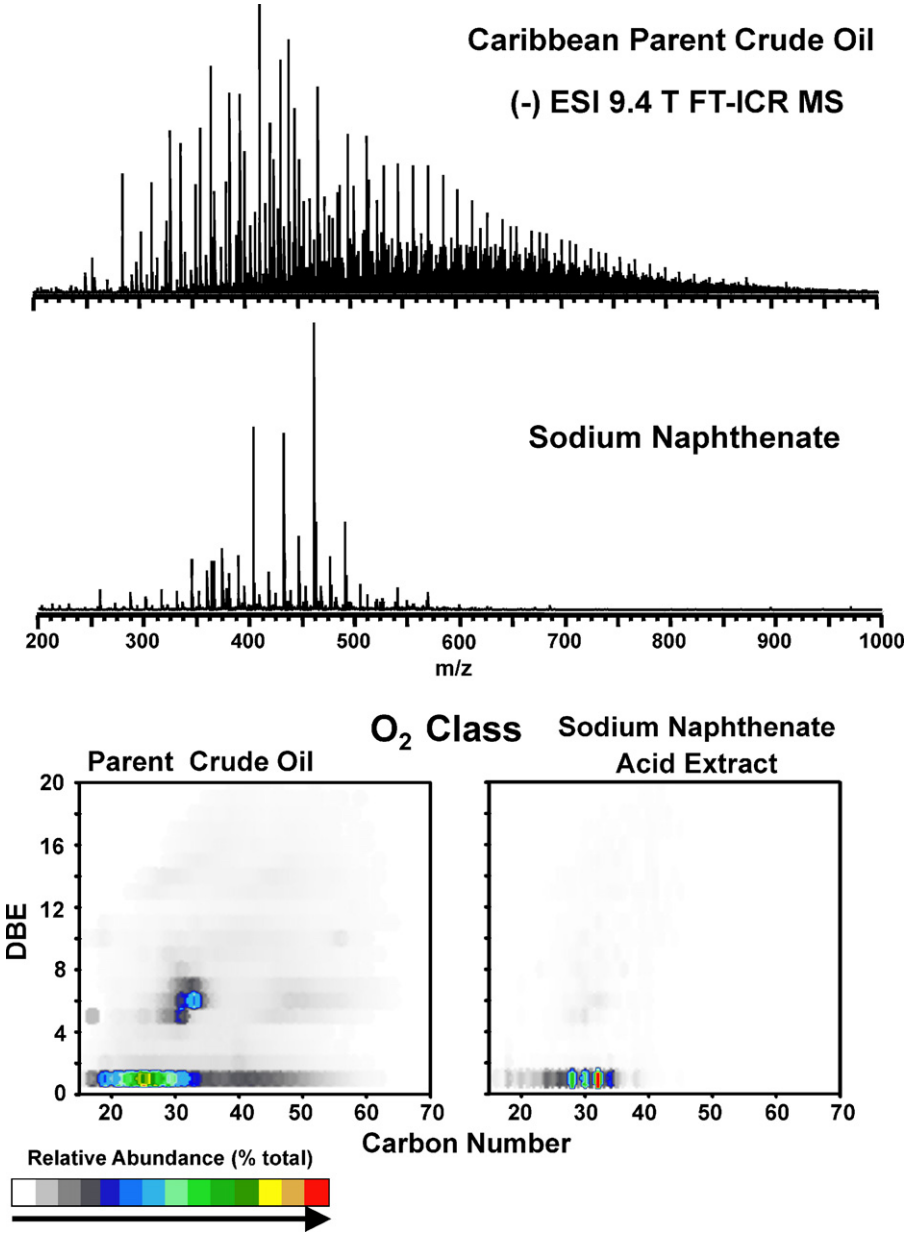

Fig. 6. Top: Broadband negative-ion electrospray 9.4 T FT-ICR mass spectra for a parent crude oil and acid extract from its associated sodium naphthenate emulsion or soap [36]. Bottom: DBE vs. carbon number images for O_2 class species from parent crude oil (left) and extract from sodium naphthenate (right).

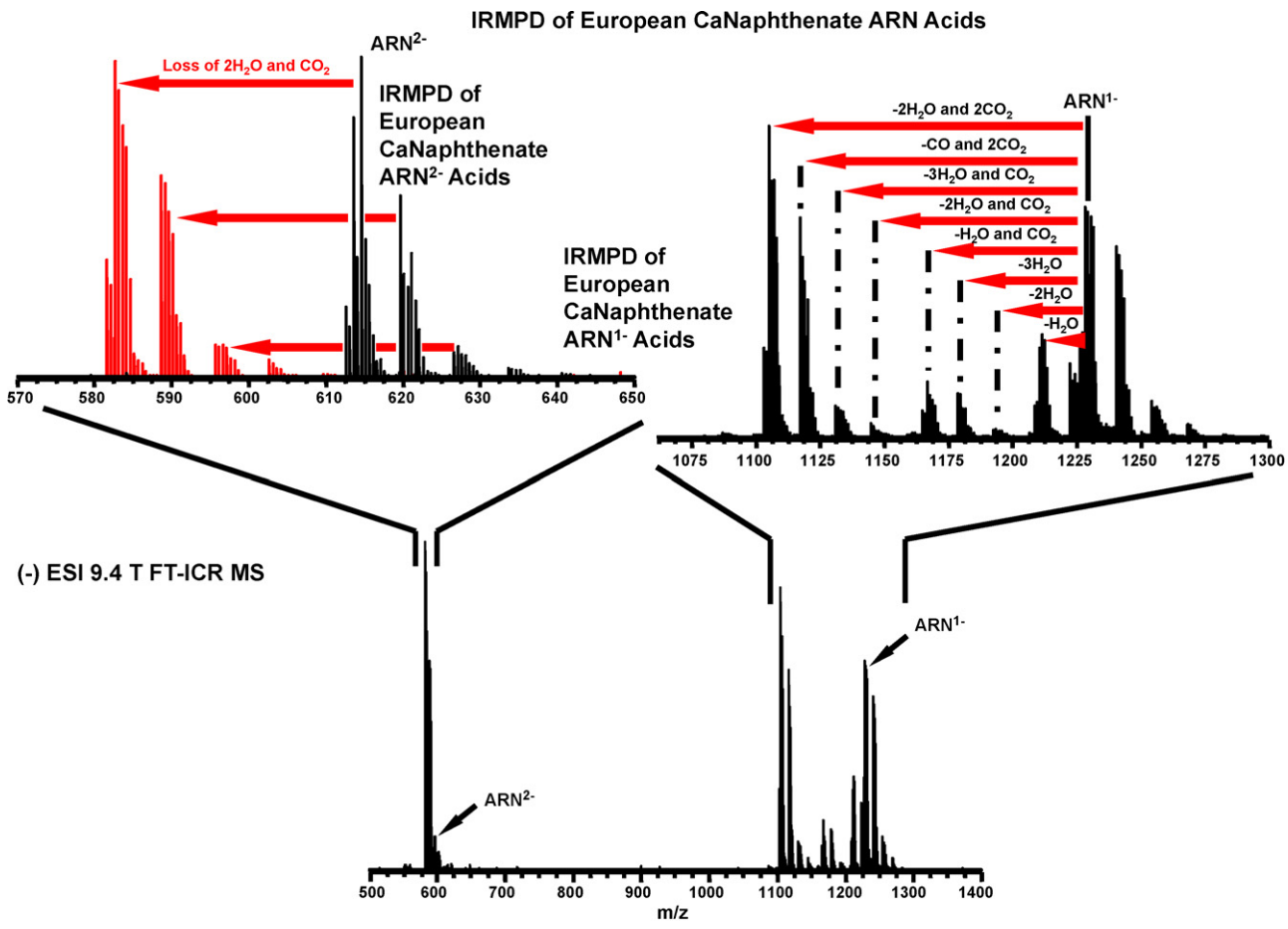

Fig. 7. Bottom: broadband negative-ion electrospray FT-ICR mass spectrum following IRMPD (low power) of ARN acids extracted from a European calcium naphthenate deposit [36]. Top: Mass scale-expanded segments following IRMPD of doubly charged (left, $570 < m/z < 650$) and singly charged (right, $1075 < m/z < 1300$) ARN acids from the same deposit. (For ARN^{2-}, the acids are in red and the IRMPD products in black.) For both ARN^{-} and ARN^{2-}, IRMPD fragmentation results in dehydration and decarboxylation of the carboxylic acids without dealkylation.

much lower acidic oxygenated class levels. Negative-ion electrospray can efficiently ionize neutral nitrogen species in a complex sample such as a crude oil without any need to preconcentrate or derivatize compounds in the sample. The Angola crude and bitumen samples exhibit mainly oxygen-containing compounds (O, OS, O_2, O_2S, O_2S_2, O_3, O_3S, O_3S_2, O_4, and O_4S) but none or lower levels of the neutral nitrogen-containing species.

In comparing relative abundances in negative-ion electrospray MS, it is important to understand that the most acidic components (in petroleum, carboxylic acids with $pK_a \sim 9$–12 in organic solvents (vs. ~4–5 in water)) will lose a proton much more easily than less acidic neutral nitrogen compounds ($pK_a \sim 20$–23) in organic solvents [37,54]. Thus, carboxylic acids will dominate the negative-ion electrospray mass spectrum (even if neutral nitrogen compounds are present in comparable quantity); conversely, if the spectrum is dominated by neutral nitrogen species, then carboxylic acids must be very low in absolute (as well as relative) abundance.

The O_2 species in petroleum and bitumen are presumably carboxylic ("naphthenic") acids. Their high relative abundance in Angola crude and Athabasca bitumen suggests extensive biodegradation. Naphthenic acids are common constituents in young and immature crude oils [13–15,17] whereas in heavy crude oils they are the original constituents of the oil and retain biomarker skeletons such as hopanes even after biodegradation [37]. However, most of the acids are formed by chemical or biochemical oxidation of the original crude oil after migration into the reservoir. Furthermore, the composition of oxygenated species in crude oil may reveal the origin of the biomass in the source rock and whether or not the petroleum formation was under oxic environment during diagenesis [37]. Even though we do not have actual total acid number (TAN (mg KOH/g of oil)) values for the three crudes, our negative-ion electrospray results suggest an acidity ranking: off-

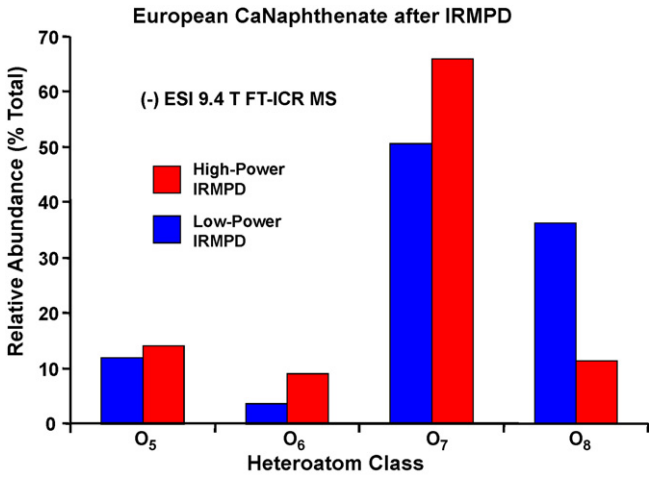

Fig. 8. Heteroatom class distribution for IRMPD (high and low power) products from singly charged ARN acids extracted from a European CaNaphthenate deposit. Only classes with relative abundance > 1% are shown.

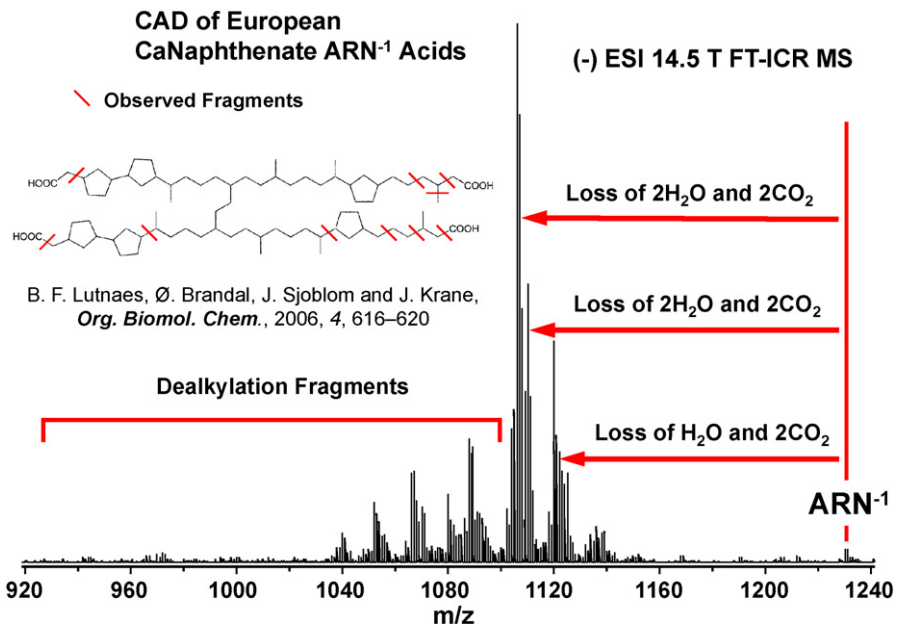

Fig. 9. Broadband negative-ion electrospray FT-ICR mass spectrum following CID of singly charged ARN acid species extracted from a European calcium naphthenate deposit. At high normalized collision energy, CID fragmentation results in dehydration and decarboxylation of the carboxylic acids with extensive fragmentation of alkyl carbons.

shore Canadian « Athabasca bitumen < Angola crude. O_4 are likely dicarboxylic acids, and further confirm the increased acidity of the two crudes. Athabasca bitumen has a high sulfur content as evidenced by the presence of six sulfur-containing classes that are mostly oxygenated. The O_oS_s classes ($o \geq 2$ and $s = 1$ or 2) presumably contain carboxylic acids, because electrospray does not deprotonate thiophenic sulfur.

3.1.3. DBE vs. carbon number distributions

Fig. 4 shows relative isoabundance color-contoured plots of DBE (a measure of aromaticity) vs. number of carbons for the N and NO_2 classes for the three samples. Based on the observed DBE range, the N class (seen only in the offshore Canadian crude) most likely comprises carbazoles (DBE = 9) or benzocarbazole (DBE = 12) homologues. The other two samples are high in the more efficiently deprotonated carboxylic acids. The high carbon number for those N species suggests extensive alkyl substitution, $(CH_2)_n$, extending from the aromatic cores of carbazoles, benzocarbazoles, dibenzocarbazoles, etc. The NO_2 class is present in all three samples, presumably rendered observable by a carboxyl moiety. The high relative abundance of the NO_2 species suggests that they could be monocarboxylic carbazoles or benzocarbazoles or dibenzocarbazoles. Possibilities for DBE = 13–15 N_1 species are: DBE = 13–14 could be benzocarbazole with either 1 or 2 rings or double bonds; DBE = 15 could be a dibenzocarbazole.

Fig. 5 shows DBE vs. carbon number images for the O_2 and O_4 classes. The O_2 species range from DBE = 1 (saturated fatty acids, in which the double bond is from the carbonyl carbon), DBE = 2,3 (non-aromatic acids), and DBE up to 20 (polyaromatic acids), with dramatic differences between offshore Canadian crude vs. the other two samples. The O_4 class (presumably dicarboxylic acids) is observed only for the most acidic samples (Angola crude and bitumen). The dicarboxylic acids are presumably readily deprotonated, and thus must be essentially absent in the offshore Canadian crude. (Monocarboxylic acid proton-bound dimers have DBE = 1 [55]. O_4 species of DBE = 1 are not seen in Fig. 5. Hence it is likely that O_4 species have a greater carbon number or hydrocarbon skeleton to accommodate the two carboxyl groups.)

3.2. Naphthenates

3.2.1. Sodium naphthenates

Both sodium and calcium naphthenates have been extensively characterized by negative-ion ESI MS [8,12,36,56]. It is possible to fingerprint a parent crude oil and link it to the suspected naphthenate deposit [36]. Fig. 6 shows broadband negative-ion ESI 9.4 T FT-ICR mass spectra of a parent crude oil (top, 200–1000 Da) and an acid extract from its associated sodium naphthenate emulsion (middle, 200–600 Da). Naphthenic acids (O_2 class) with DBE = 1 in the parent crude oil (Fig. 6, bottom left) are selectively enriched in the sodium naphthenate emulsion (Fig. 6, bottom right), because their surfactant-like structures (polar carboxylic head and non-polar aliphatic tail) enhance their ability to bind to monovalent cations in oil/aqueous brine systems [36]. The parent crude oil also contains naphthenic acids of DBE = 5–7, presumably hopanoic acids. Crude oils that are highly biodegraded are likely to form sodium naphthenate emulsions, but are likely to contain cycloalkane/aromatic ring moieties that decrease their ability to bind to monovalent cations (relative to fatty acid-like naphthenic acids), so that they are not present in the acid extract from a sodium naphthenate emulsion.

3.2.2. Calcium naphthenates

Negative-ion ESI FT-ICR mass spectra of acid extracts from calcium naphthenate deposits exhibit two narrow peaks arising from ARN acids: singly charged $[M-H]^-$ ions of m/z 1225–1270 and doubly charged $[M-2H]^{2-}$ ions of m/z 615–630 [36]. Doubly charged ARN acids $[C_{80}H_{142}O_8\text{-}2H]^{2-}$ are formed by deprotonation of two of the carboxylic groups in the parent compound $C_{80}H_{142}O_8$, whereas singly charged ARN $[C_{80}H_{142}O_8\text{-}H]^-$ are from deprotonation of one of the four carboxylic acid groups in the parent compound [36]. The most abundant singly charged ion, at 1230.06293 Da, corresponds to the molecular formula, $[C_{80}H_{142}O_8\text{-}H]^-$.

CID and IRMPD experiments provide structural characterization of the ARN acids. Fig. 7 (bottom) shows a broadband negative-ion ESI 9.4 T FT-ICR mass spectrum following IRMPD fragmentation of an ARN acid extract from a calcium naphthenate deposit. Infrared irradiation of the parent compound results in multiple decar-

boxylation and dehydration of the carboxylic groups (see mass scale-expanded segments in Fig. 7, top). Infrared irradiation of the singly charged ARN acids results in the loss of up to three carboxyl groups, consistent with the proposed tetracarboxylic acid functionality [9]. Loss of up to 2–3 H_2O molecules was also observed. The fourth decarboxylation is not observed because its removal leaves a neutral product.

The O_n, n = 5–8, distribution for products of low- and high-power IRMPD of the singly charged ARN acids from a calcium naphthenate deposit is shown in Fig. 8. The O_8 species are the singly charged parent ARN acids. High IRMPD power increases fragmentation of the singly charged ARN acids.

CID of the singly charged ARN acids resulted in dehydration and decarboxylation (see Fig. 9) similar to that from IRMPD. Based on the structure proposed by Lutnaes et al. [9], we were able to assign fragments spanning all four "talons" of the ARN acid, including the loss of one and two cyclopentane rings. Fragments retained 1 to 3 rings based on their DBE values. Fragmentation of the individual cyclopentane rings was not observed.

Acknowledgments

This work is dedicated to John B. Fenn, and was supported by NSF Division of Materials Research through DMR-0654118 and the State of Florida. We thank Brandie Erhmann for providing FT-ICR MS data for offshore Canadian crude oil.

References

[1] M.I. Head, M.D. Jones, R.S. Larter, Nature 426 (2003) 344–352.
[2] K.H. Altgelt, M.M. Boduszynski, Composition and Analysis of Heavy Petroleum Fractions, 1994.
[3] A.G. Marshall, R.P. Rodgers, Acc. Chem. Res. 37 (2004) 53–59.
[4] R.P. Rodgers, T.M. Schaub, A.G. Marshall, Anal. Chem. 77 (2005) 20A–27A.
[5] A.G. Marshall, R.P. Rodgers, PNAS 105 (2008) 18090–18095.
[6] M. Turner, C.P. Smith, Paper No. SPE 94339 2005.
[7] J.E. Vinstad, A.S. Bye, K.V. Grande, B.M. Hustad, B. Nergard, Paper No. SPE 80375 2003.
[8] D.L. Gallup, J.A. Curiale, P.C. Smith, Energy Fuels 21 (2007) 1741–1759.
[9] B.F. Lutnaes, O. Brandal, J. Sjoblom, J. Krane, Org. Biomol. Chem. 4 (2006) 616–620.
[10] B. Brocart, C. Hurtevent, J. Dispersion Sci. Technol. 29 (2008) 1496–1504.
[11] T.D. Baugh, N.O. Wolf, H. Mediaas, J.E. Vinstad, K.V. Grande, Paper No. SPE 93111, 2005.
[12] B.F. Lutnaes, J. Krane, B.E. Smith, S.J. Rowland, Org. Biomol. Chem. 5 (2007) 1873–1877.
[13] T.D. Baugh, N.O. Wolf, H. Mediaas, J.E. Vinstad, K.V. Grande, Prepr.-Am. Chem. Soc., Div. Pet. Chem. 49 (2004) 274–276.
[14] S.D. Olsen, Prepr.-Am. Chem. Soc., Div. Pet. Chem. 43 (1998) 142–145.
[15] T. Barth, L.K. Moen, C. Dyrkorn, Prepr.-Am. Chem. Soc., Div. Pet. Chem. 3 (1998) 134–136.
[16] P.C. Smith, Soaps (Naphthenates) Scales Management from Deepwater Flow Assurance Aspects to Oil Terminal Sludge Processing Workshop. In Flow Assurance-A Holistic Approach, Kuala Lumpur, Malaysia, December 2004; International Quality and Productivity Center.
[17] D.L. Gallup, Ca-Naphthenates and Metallic Soap Deposits: Formation and Mitigation. In Flow Assurance-A Holistic Approach, Kuala Lumpur, Malaysia, December 2004; International Quality and Productivity Center.
[18] O. Brandal, T. Viitala, J. Sjoblom, J. Dispersion Sci. Technol. 28 (2007) 95–106.
[19] A.M. Hanneseth, O. Brandal, J. Sjoblom, J. Dispersion Sci. Technol. 27 (2006) 185–192.
[20] J. Saab, I. Mokbel, A.C. Razzouk, N. Ainous, N. Zydowicz, J. Jose, Energy Fuels 19 (2005) 525–531.
[21] J.B. Fenn, M. Mann, C.K. Meng, S.F. Wong, C.M. Whitehouse, Science 246 (1989) 64–71.
[22] J.B. Fenn, Angew. Chem. Int. Ed. 42 (2003) 3871–3894.
[23] D.L. Zhan, J.B. Fenn, Int. J. Mass Spectrom. Ion Proc. 194 (2000) 197–208.
[24] S.D. Fuerstenau, W.H. Benner, Rapid Commun. Mass Spectrom. 9 (1995) 1528–1538.
[25] S.D. Fuerstenau, W.H. Benner, J.J. Thomas, C. Brugidou, B. Bothner, G. Suizdak, Angew. Chem. Int. Ed. 40 (2001) 541–544.
[26] N. Felitsyn, M. Peschke, P. Kerbale, Int. J. Mass Spectrom. 219 (2002) 39–62.
[27] J. Chmielowiec, P. Fischer, C.M. Pyburn, Fuel 66 (1987) 1358–1363.
[28] V. LaVopa, C.N. Satterfield, J. Catal. 110 (1988) 375–387.
[29] B. Wen, M. He, C. Costello, Energy Fuels 16 (2002) 1048–1053.
[30] W.K. Seifert, R.M. Teeter, Anal. Chem. 42 (1970) 750–758.
[31] E. Slavcheva, B. Shone, A. Turnbull, Brit. Corros. J. 34 (1999) 125–131.
[32] S.K. Panda, J.T. Andersson, W. Schrader, Angew. Chem. Int. Ed. 48 (2009) 1788–1791.
[33] J.M. Purcell, P. Juyal, D.G. Kim, R.P. Rodgers, C.L. Hendrickson, A.G. Marshall, Energy Fuels 21 (2007) 2869–2874.
[34] N.B. Cech, C.G. Enke, Mass. Spec. Rev. 20 (2001) 362–387.
[35] C.G. Enke, Anal. Chem. 69 (1997) 4885–4893.
[36] M.M. Mapolelo, L.A. Stanford, R.P. Rodgers, T.A. Yen, J.D. Debord, S. Asomaning, A.G. Marshall, Energy Fuels 23 (2009) 349–355.
[37] C.A. Hughey, R.P. Rodgers, A.G. Marshall, K. Qian, W.K. Robbins, Org. Geochem. 33 (2002) 743–759.
[38] M.R. Emmett, F.M. White, C.L. Hendrickson, S.D.H. Shi, A.G. Marshall, J. Am. Soc. Mass Spectrom. 9 (1998) 333–340.
[39] M.W. Senko, J.D. Canterbury, S. Guan, A.G. Marshall, Rapid Commun. Mass Spectrom. 10 (1996) 1839–1844.
[40] G.T. Blakney, G. Van der Rest, J.R. Johnson, M.A. Freitas, J.J. Drader, S.D.-H. Shi, C.L. Hendrickson, N.L. Kelleher, A.G, Marshall, In *Further Improvements to the MIDAS Data Station for FT-ICR Mass Spectrometry*; Proceedings of the 49th American Society for Mass Spectrometry Conference on Mass Spectrometry and Allied Topics, Chicago, IL, May 2001; p WPM 265.
[41] M.W. Senko, C.L. Hendrickson, M.R. Emmett, S.D.H. Shi, A.G. Marshall, J. Am. Soc. Mass Spectrom. 8 (1997) 970–976.
[42] B.E. Wilcox, C.L. Hendrickson, A.G. Marshall, J. Am. Soc. Mass Spectrom. 13 (2002) 1304–1312.
[43] C.L. Hendrickson, J.P. Quinn, M.R. Emmett, A.G. Marshall, In *Quadrupole Mass Filtered External Accumulation for Fourier Transform Ion Cyclotron Resonance Mass Spectrometry*; 48th American Society for Mass Spectrometry Conference on Mass Spectrometry and Allied Topics, Long Beach, CA, 2000; p MPB 083.
[44] E.B.J. Ledford, D.L. Rempel, M.L. Gross, Anal. Chem. 56 (1984) 2744–2748.
[45] S.D.H. Shi, J.J. Drader, M.A. Freitas, C.L. Hendrickson, A.G. Marshall, Int. J. Mass Spectrom. 195/196 (2000) 591–598.
[46] L.L. Lopez, P.R. Tiller, M.W. Senko, J.C. Schwartz, Rapid Commun. Mass Spectrom. 13 (1999) 663–668.
[47] E. Kendrick, Anal. Chem. 35 (1963) 2146–2154.
[48] C.A. Hughey, C.L. Hendrickson, R.P. Rodgers, A.G. Marshall, K. Qian, Anal. Chem. 73 (2001) 4676–4681.
[49] C.A. Hughey, C.L. Hendrickson, R.P. Rodgers, A.G. Marshall, Energy Fuels 15 (2001) 1186–1193.
[50] R. Jaffe, M.T. Gallardo, Org. Geochem. 20 (1993) 973–984.
[51] L.R. Nascimento, L.M.C. Rebooucas, L. Koike, F.D.M. Reis, A.L. Soldan, Org. Geochem. 30 (1999) 1175–1191.
[52] F.W. McLafferty, F. Turecek, Interpretation of Mass Spectra, 4th ed., University Science Books, Mill Valley, CA, 1993.
[53] N.A. Tomczyk, R.E. Winans, J.H. Shinn, R.C. Robinson, Energy Fuels 15 (2001) 1498–1504.
[54] F.G. Bordwell, Acc. Chem. Res. 21 (1988) 456–463.
[55] R. Zhang, C. Lifshitz, J. Phys. Chem. 100 (1996) 960–966.
[56] B. Brocart, M. Bourrel, C. Hurtevent, J.-L. Volle, B. Escoffier, J. Dispersion Sci. Technol. 28 (2007) 331–337.